Charge-coupled device imaging of rapid calcium transients in cultured arterial smooth muscle cells

J. J. LINDERMAN[1,2], L. J. HARRIS[2,*], L.L. SLAKEY[2] and D. J. GROSS[2]

[1] Department of Chemical Engineering, University of Michigan Ann Arbor, Michigan, USA
[2] Department of Biochemistry and Program in Molecular and Cellular Biology, University of Massachusetts, Amherst, Massachusetts, USA

Abstract — Transient changes in the concentration of intracellular free calcium are associated with the transduction of primary signals and the subsequent employment of Ca^{2+} as a second messenger in a multitude of cell types. These transients, typically monitored with the calcium-sensitive fluorescent dye Fura-2, are known to occur with a time course in the order of seconds. In order to accurately monitor such rapid changes in intracellular free calcium concentration in both single cells and simultaneously in several cells in a single field, we have developed a digital fluorescence imaging system based on a charge-coupled device (CCD) camera. We report here on the detailed kinetics of calcium increases in cultured arterial swine smooth muscle cells in response to the agonist ATP.

A variety of studies has implicated the calcium ion as a second messenger in the transduction of a variety of primary signals. The treatment of both transformed and untransformed cells with agonists such as nucleotides, hormones, growth factors, and neurotransmitters has been shown to result in a stimulated increase in the concentration of cytosolic free calcium. Several studies have shown that the source of this calcium may be the extracellular medium, suggesting the opening of plasma membrane calcium channels as a part of the response to agonist [1-3], and/or the release of intracellular stores of calcium, a response which occurs in the absence of extracellular calcium [2-6]. In smooth muscle cells, the intracellular stores of calcium are located in the sarcoplasmic reticulum (SR), and some agonists can stimulate the release of

calcium from these stores [7-9].

A variety of techniques has been used to measure both steady state and transient cytosolic calcium ion concentrations. Populations of adherent or suspended cells loaded with the fluorescent calcium indicator Fura-2 and examined using a fluorometer showed that the cell population as a whole may respond to agonists with a calcium transient that rises in a few seconds and then falls back to a baseline concentration or to an elevated

---

---

* Present address: Radiology Department, University of Massachusetts Medical Center, 55 Lake Avenue N, Worcester, MA 01605, USA

E

concentration over a period of minutes [1, 3]. The measurement of sub-second kinetics of the calcium response in Fura–2 loaded platelets using stopped-flow fluorometry demonstrated that the population responds to a variety of agonists with a calcium rise in less than one second [5]. Data may also be obtained from single cells using photomultiplier [10] or imaging techniques [11]; stimulated calcium transients in single cells occur rapidly as well [2, 6, 12]. For example, the intracellular calcium concentrations of individual BC3H-1 muscle cells stimulated with phenylephrine were observed to oscillate with a frequency of approximately 2 min^{-1} [13]. Thus it is evident that transients in the concentration of intracellular free calcium may be rapid, occurring in the order of a few seconds or less.

We have developed a quantitative digital fluorescent imaging system based on a charge-coupled device (CCD) camera that can resolve rapid calcium transients in single cells. Multiple cells within the same field of view can be imaged simultaneously, allowing temporal and spatial measurement of the free calcium concentration within each cell. The use of a CCD as an imag- ing device offers several advantages: linearity, high resolution, photometric accuracy, and geometric stability [14, 15]. In addition, the user may elect to reduce spatial resolution and/or the size of the area that is imaged to gain imaging speed or to use the CCD as an image storage device, as detailed below.

To accurately determine the intracellular calcium concentration at a point in time using the calcium-sensitive fluorescent indicator Fura–2, a pair of images of the same field must be obtained, each one taken at a different excitation wavelength. Our system is designed to collect these two images with very little time between the two exposures, thereby minimising errors of temporal registration for rapidly changing signals. The time required to collect and store a pair of images increases with image size and exposure time. As detailed later, the minimum time between the two wavelength images is 200 ms.

Using our digital fluorescence imaging system, we have examined the detailed kinetics of transients in intracellular calcium concentration in individual cultured arterial smooth muscle cells (SMC) stimulated with ATP. ATP, which acts as a constrictor in some smooth muscle beds and as a relaxant in others [16], is co-released with several neurotransmitters [17]. It may also be released from stimulated platelets [18]. Slakey [19] estimated that ATP may reach smooth muscle cells and neighbouring endothelial cells at micromolar concentrations. An ATP-induced rise in intracellular free calcium has been observed in populations of suspended rat aortic smooth muscle cells [20] while isolated arterial smooth muscle cells from rabbit ear have been shown to contain an ATP-activated Ca^{2+}-permeable ion channel [21]. In the present study, we have examined the ATP-stimulated transients in intracellular free calcium in individual adherent SMC from pig aorta.

Materials and Methods

Cell and flow chamber preparation

Smooth muscle cells from pig aortas were isolated and cultured as described previously [22]. Briefly, medial tissue was minced into 1 mm pieces and incubated in Dulbecco's modified Eagles medium (DME; Gibco, Grand Island, NY, USA) supplement-ed with 0.3% collagenase at 37°C for 4 h. The digest was then centrifuged and the pellet resuspended in growth medium one (GM1), consisting of DME, formulation 43-1600 as supplied by Gibco, and supplemented with 3.5 g/l additional glucose (4.5 g/l total glucose), 4 mM glutamine, non-essential amino acids' solution for MEM as supplied by Gibco, 200 U/ml penicillin, 0.2 mg/ml streptomycin, 0.6 mg/ml tylocine, and 10% fetal calf serum, and placed in a T-25 flask. Cells attached and grew to confluence within 7 to 10 days. Cells were then subcultured in growth medium two (GM2; identical to GM1 except for the omission of tylocine, non-essential amino acids, and the reduction of the glucose concentration to 1 g/l total) for 2 to 3 passages before use. Approximately 2–3 days before an experiment, the cells were returned to GM1.

Coverslips were prepared by placement of a few drops of a dilute fibronectin solution (gift from the laboratory of E. Westhead) on No. 1 glass coverslip surfaces, incubation of the coverslips at 37°C and

5% CO_2 for at least 30 min, and subsequent removal of the solution from the surface by suction. Adherent cells were removed from confluent flasks by treatment with 0.05% trypsin/versene solution and were plated at approximately a 1:2.5 dilution onto fibronectin-coated coverslips in GM1. This cell dilution was chosen to ensure subconfluence at the time of imaging, so that individual cells could easily be distinguished. Cells were incubated overnight, and the following day the cells were rinsed and the medium was changed to a serum-free defined medium (DM) containing DME supplemented as described by Libby and O'Brien [23]. Cells were cultured in this serum-free medium for 24 h.

Cells on coverslips were loaded with calcium-sensitive dye by a 30 min incubation at 37°C in a 5% CO_2 atmosphere with Fura–2 acetoxymethly ester (Fura–2/AM; Molecular Probes, Eugene, OR, USA). The Fura–2/AM was dissolved in dry dimethylsulfoxide (DMSO) at a stock concentration of 1 mM and mixed with DM to a concentration of 2 μM Fura–2/AM and 0.1% DMSO. Each coverslip contained approximately 10^5 cells; the total volume of DM containing Fura–2/AM that was applied to the coverslip was 1.5 ml. Coverslips were then rinsed several times with HEPES-buffered saline (HBS; 20 mM HEPES, 125 mM NaCl, 5.4 mM KCl. 1.8 mM $CaCl_2$, 0.8 mM $MgSO_4$, 5.5 mM D-glucose), mounted in a flow chamber, and viewed immediately. Cells examined for autofluorescence were not incubated with Fura–2/AM but were otherwise prepared in an identical fashion.

The flow chamber (Fig. 1) consisted of a 6 mm thick stainless steel plate with a vertical hole 13 mm in diameter through its centre. The coverslip containing the SMC was placed in a shallow slot on the bottom face of the plate and secured using petroleum jelly. A clean coverslip was mounted on the top face of the plate and anchored in place using a molten 1:1:1 mixture of petroleum jelly, lanolin and paraffin, thus forming a cylindrical chamber with a volume of approximately 0.8 ml. The flow chamber allows gravity-fed flow in from a 1.5 ml reservoir above and to one side of the chamber, through a 1.5 mm diameter hole drilled at an angle through the plate and ending just above the coverslip covered with cells, and out through a small channel at the top of the chamber on the side opposite from the inlet. A small tube applied continuous suction to remove any excess fluid. A thin copper plate was placed beneath the flow chamber to help support the coverslip and to aid in heat conduction.

Cells and the surrounding medium in the flow chamber were maintained at 37°C. A circulating constant temperature water bath pumped water through copper tubing wrapped around the objective lens and through copper tubing soldered to a copper temperature stage. The copper stage was insulated from the microscope stage by Teflon spacers, and the cell-covered coverslip in the flow chamber was placed directly over the objective through an opening in the temperature stage.

Agonist introduction

Stimulants were introduced into the flow chamber by injection of approximately 2.5 ml of a 37°C solution of the agonist in HBS into the flow chamber reservoir. The addition took 2–3 s, and one chamber volume of solution flowed into the chamber within 2 s of the start of the injection. ATP was obtained from Sigma (St Louis, MO, USA). The non-fluorescent calcium ionophore Br-A23187 was obtained from Molecular Probes.

Instrumentation

A schematic of the imaging system is shown in Figure 1. The fluorescence epi-illumination system is based on a 75 watt Hg-Xe arc lamp (Hamamatsu Corp., Bridgewater, NJ, USA) and a pair of monochromators (model H20, Instruments SA Inc., Metuchen, NJ, USA, each equipped with a KM 524.00.230 1200 g/mm grating blazed at 330 nm), the latter used in place of interference filters to allow convenient tuning of excitation wavelengths [10]. The lamp was chosen for its stability and long life in addition to its high brightness at the Hg spectral lines of 334 and 365 nm. We chose to employ monochromators rather than interference filters primarily for the ease of tuning that the monochromators provide. Although we commonly use the Hg spectral lines for fluorescence excitation,
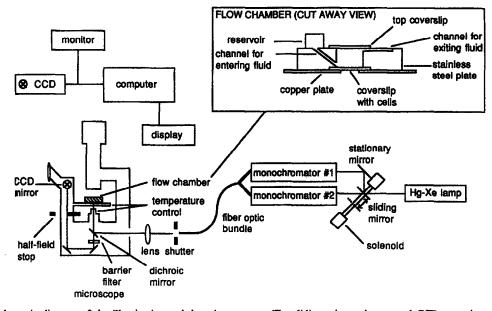
Fig. 1 Schematic diagram of the illumination and detection system. The sliding mirror, shutter, and CCD operation are computer controlled. Inset: Schematic diagram of the flow chamber

all intermediate wavelengths are easily accessible by a simple turn of the monochromator tuning knob. Additionally, the spectral transmission properties of the monochromators are variable by the choice of entrance and exit slits. For Fura–2 imaging the upper monochromator was set to 365 nm center wavelength with an entrance slit of 2 mm while the lower monochromator center wavelength was set to 334 nm with a 4 mm entrance slit. As the exit port of each monochromator was coupled a rectangular cross section fiber optic bundle of 2 mm width (see Fig. 1 and below), the upper monochromator had a triangular bandpass profile peaked at 365 nm of 8 nm width at half maximum transmission with nearly zero transmission below 357 nm or above 373 nm. The lower monochromator had a trapezoidal bandpass profile centered at 334 nm of 16 nm width at half maximum transmission and nearly zero transmission below 320 nm and above 348 nm. According to the manufacturer's specifications, the relative overlap of the two spectral regions chosen for Fura–2 excitation is $<10^{-5}$. Although we have done no direct comparisons between our monochromators and interference filters, it is possible in theory to obtain more light from a monochromator than from an interference filter. In practice, the size of the diffraction grating and

optics associated with the monochromator as well as the wavelength dispersion of the grating determine the transmission efficiency of the monochromator. A straightforward discussion of monochromators can be found in [24]. Fluorescence excitation of the cells therefore occurs at 334 nm and 365 nm, corresponding to two spectral lines of the Hg-Xe arc. When the sliding mirror is moved out of the light path, light is directed into the lower monochromator. A solenoid drive under computer control stably repositions the mirror in under 200 ms.

The exit ports of both monochromators were directly coupled to the two ends (2 mm wide by 8 mm high) of a 51 cm long bifurcated quartz fiber optic bundle (Volpi Manufacturing USA, Auburn, NY, USA) which terminates in a 6.4 mm diameter circular cross section randomised bundle directing the light through a computer controlled electronic shutter (A.W. Vincent Associates, Inc., Rochester, NY, USA) with an open/close time of less than 5 ms. According to data from Volpi Manufacturing, the transmissivity of this length of fiber is 60% from 900 to 450 nm, dropping to 55% at 300 nm. After passing through a 75 mm focal length fused silica biconvex lens, the light entered the epi-illumination port of a Zeiss IM-35 inverted microscope (Carl

Zeiss, Inc., Thornwood, NY, USA) equipped with quartz epi-illumination optics and a Nikon 40x/1.3 NA CF Fluor UV lens (Nikon Inc. Instrument Division, Garden City, NJ, USA). A Zeiss FT 395 dichroic mirror and a flow fluorescence long-pass barrier filter with 50% cutoff at 399 nm (Schott Glass Technologies, Duryea, PA, USA) completed the fluorescence system.

Images were detected by a CCD instrumentation camera (Photometrics, Ltd., Tuscon, AZ, USA) equipped with a 390 x 584 pixel Texas Instruments 4849 CCD chip thermoelectrically cooled to approximately –45°C to reduce thermal noise. The chip allows image collection at very high quantum efficiencies (20–60% at visible wavelengths) with a high degree of linearity and low readout noise (in the order of 15 photoelectron equivalents). The analog image is digitised to 12 bit resolution and was transmitted to the computer via a 500 kHz IEEE-488 interface (National Instruments, Austin, TX, USA).

Computer control of the illumination system (mirror placement, shutter opening and closing) and the CCD camera was accomplished via a Masscomp 5500 computer (Concurrent Computer Corp., Oceanport, NJ, USA). A 14 Mflop Masscomp array processor enhances image computations during and after data collection. A Masscomp GA-1000 graphics subsystem, which included a pair of 1152 x 910 by 12 bit deep image planes and an independent graphics processor, was used for image display. Because 2 of the bit planes were used for overlay graphics, 10 bit planes are available for high resolution image display.

Operation of the CCD

The CCD may be operated in one or more of several specialised modes, as shown in Figure 2. Straightforward operation allows a full-frame 390 x 584 image to be collected on and read from the CCD chip; the time required to digitise and store the full frame is approximately 1.5 s. Alternatively, data may be read from a portion (or subarray) of the entire field; the readout and storage time is reduced from the time for a full-frame readout and storage approximately in proportion to the size of the subarray chosen. The operation of the CCD in subarray mode thus allows the same lateral resolution as a full-frame image, although over a smaller area of the field.

The CCD is also programmed to bin or combine, the photoelectrons contained in adjacent pixels at the time of readout, prior to digitisation. Binning 2 x 2, for example, combines the charge of 2 pixels in the x-direction and 2 pixels in the y-direction to form an array of 'superpixels'. The readout time for a binned image is reduced from the full frame, unbinned image readout time in proportion to the size of the final image – i.e. a 2 x 2 binned image takes approximately 1/4 the readout time of a full frame image. Since a major source of image noise is generated during image readout, combining pixel charge before readout produces a superior signal to noise ratio in the final image as compared to an unbinned image or to an image which is binned to the same degree after readout. The spatial resolution of a binned image is necessarily reduced.

Third, the CCD can be operated in frame transfer mode. In this mode, the CCD operates simultaneously as both a photoelectron storage and collection device. Half of the field of view is physically masked by placing a partial field stop between the specimen and the CCD in a focal plane conjugate to the image plane. An image of the visible half of the field is collected by illumination at one excitation wavelength. After closing the shutter, the collected image is electronically shifted from the unmasked half of the CCD chip to the masked half in under 1 ms. A second image of the same half of the field is then collected by illumination at a second excitation wavelength. The resultant full CCD image shows the same field twice, once for each excitation wavelength (*see* Fig. 2).

Image collection software

Image collection and processing was accomplished through menu-driven software modified from a base system, Vista-IPS (Paragon Imaging, Lowell, MA, USA). Time-lapse imaging is accomplished via a set of programs that can direct the collection of up to 1000 images of three separate types (i.e. frame transfer, binned, brightfield, etc) at a user-specified frequency. During image collection, images may be displayed on a monitor (Sanyo Electric, Inc.,
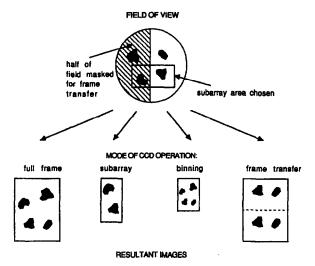
FIELD OF VIEW

half of
field masked
for frame
transfer

subarray area chosen

MODE OF CCD OPERATION:

full frame   subarray   binning   frame transfer

RESULTANT IMAGES

Fig. 2 Modes of operation of the CCD. The CCD may be used to take a full frame 390 x 584 pixel image or a smaller subarray. Binned images may be collected by combining the charge on neighbouring pixels at the time of readout. Frame transfer imaging allows the collection of two separate images of the same field of view on the partially masked CCD chip before the chip is read

Compton, CA, USA) connected to the CCD camera on the graphics terminal. The latter display is available for concurrent display and image analysis.

Image collection and processing

Fluorescence images of cells at the two excitation wavelengths were collected using the CCD frame transfer mode of operation, as described above. Because the SMC spread very thinly on the coverslip surface, typical operation of the CCD with no binning requires a 2000 ms exposure at 334 nm and a 200 ms exposure at 365 nm; 2 x 2 binning allowed these exposure times to be reduced by a factor of four. Blank field background images at both wavelengths were taken for each coverslip and subtracted from each of the cell images. The resultant background subtracted images were then split into halves, each half corresponding to one of the original excitation wavelengths, and ratio images (R) were generated, where $R = F_{334}/F_{365}$, the fluorescence intensity at 334 nm divided by the fluorescence intensity at 365 nm. Autofluorescence contributed only 3–5% of the total fluorescence at each of the illumination wavelengths. Computations of ratio images and subsequent processing were

carried out with floating point precision.

Calibration measurements are taken by imaging three solutions in the flow chamber positioned on the microscope stage: 10 μM Fura–2 free acid (Molecular Probes) in phosphate-buffered saline (PBS) supplemented with 2 mM $CaCl_2$, 10 μM Fura–2 free acid in PBS supplemented with 2 mM EDTA and PBS alone (for background subtraction). $R_{max} = (F_{334}/F_{365})$ at saturating Ca^{2+}, $R_{min} = (F_{334}/F_{365})$ at no Ca^{2+}, and $\beta = F_{365}$(no calcium)/F_{365}(saturating Ca^{2+}) were calculated from these images. Use of these calibration measurements led to calculated resting $[Ca^{2+}]_i$ in the order of 30 nM. As this level seemed rather low in comparison with the resting $[Ca^{2+}]$ in other cells reported in the literature [2, 6, 10, 12, 13] and in the light of the known systematic bias toward low calculated $[Ca^{2+}]_i$ when Fura–2 is in high viscosity or protein-containing media [25], we adopted a simple correction procedure to approximate the differing conditions in the cytosol as compared to PBS. All systematic bias may not be completely removed by this procedure. Corrections for intracellular viscosity were determined by imaging solutions as above but supplemented with 60% (w/v) sucrose (RY Tsien, personal communication); R_{max}, R_{min} and β are respectively found to be 60%, 95%, and 80% lower in the high viscosity solutions as compared to PBS. The viscosity-corrected β for our imaging system was approximately 1.4 and the corrected R_{min} and R_{max} were approximately 0.2 and 0.05. All three parameters vary across the field of view. Intracellular free Ca^{2+} was determined according to the equation $[[Ca^{2+}]_i = K_d\beta[(R - R_{min})/(R_{max} - R)]$, where $K_d = 224$ nM is the equilibrium dissociation constant for Ca^{2+} and Fura–2 [26].

Series of ratio or calcium images calculated as described were then processed by a masking technique to determine the average value of the fluorescence intensity ratio or calcium concentration at various regions in each cell as a function of time. Masking was performed in one of two ways. If the cell of interest did not move, and if there was no drift of the field of view during the experiment, a one bit overlay mask of a region of the cell, corresponding to pixels in the cell image above a user-set threshold grey level value and delimited
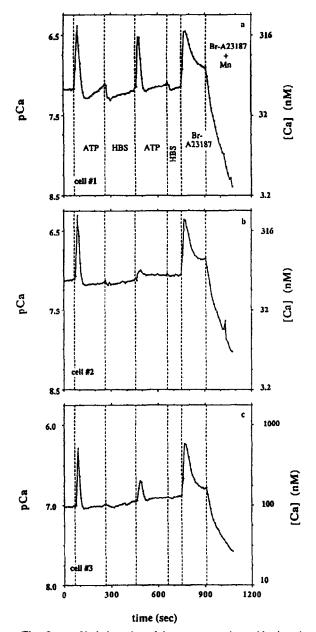
Fig. 3a–c   Variations in calcium concentration with time in response to ATP and ionophore for three cells in the same field. Agents were added (ATP, Br-A23187) or removed (HBS) at times indicated by the vertical dashed lines.   Agonist concentrations: ATP, 50 µM; Br-A23187, 1 µM; MnCl₂, 2 mM. Images were collected using frame transfer

interactively by the user to regions of interest, was made and applied to each of the images in the time-lapse sequence.   The threshold level is determined interactively by the user; typically the level was set such that the image of the cell

fluorescence illuminated at 365 nm was sharply delineated.   This usually samples the cell interior but avoids very dim cell extensions.   If there was a change in the shape or position of the cell during the experiment, the cells were masked interactively: the user selected the region of interest in each frame of the time-lapse sequence.   Pixels in the ratio or calcium image which corresponded to a division by zero in the ratio calculation were excluded during either masking procedure.

Image display in either grey levels or pseudocolour was possible.   Ratio or calcium images could be displayed at 10 bit resolution; for this display mode 5 bits of the displayed image derived from the 365 fluorescence image modulate image intensity and 5 bits derived from the ratio or calcium image modulate image colour.   This display allows the viewer to simultaneously observe calculated ratio or calcium levels as well as intrinsic fluorescence levels at all points across the cells. Correlation of deviant calculated $[Ca^{2+}]_i$ with above average or below average fluorescence brightness in a pixel or cell region is facilitated.   Data collection as described in the previous paragraph was from 32 bit floating point ratio or calcium images and was independent of image display.

Results

The application of ATP to Fura–2 loaded SMC stimulated a rise in the concentration of intracellular free calcium in the presence of extracellular calcium.   In Figure 3a–c, plots of intracellular calcium concentration versus time are shown for 3 SMC in a single 390 x 192 pixel field.   Pairs of images were collected approximately every 9 s using the frame transfer mode of CCD operation; exposure times of 2000 ms at 334 nm and 200 ms at 365 nm illumination wavelengths were used.   All three cells began with mean intracellular free calcium concentration of 70–100 nM and responded immediately and synchronously to the addition of 50 µM ATP at 75 s, with a rise to a peak of 410–520 nM calcium.   The cells returned to initial or less than initial calcium concentrations about 55 s after the initial rise.   At 270 s, the ATP was removed and cellular calcium levels dropped slightly, remaining roughly constant until a second addition of 50 µM
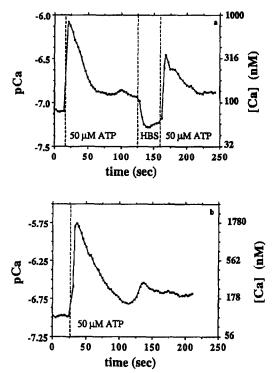
Fig. 4 (a) Variations in calcium concentration with time in response to 50 μM ATP for the cell shown in Plate 9. Addition and washout of ATP are indicated by vertical dashed lines. Note that [Ca^{2+}]$_i$ does not rise until after ATP addition. Images were collected using frame transfer, subarray, and binning capabilities. (b) Variations in calcium concentration with time in response to 50 μM ATP for a single cell. Addition of ATP is indicated by the vertical dashed line. Note that [Ca^{2+}]$_i$ does not rise until after ATP addition. Images were collected using frame transfer, subarray and binning capabilities

ATP to the chamber at 465 s. All three cells once again responded, although cells 2 and 3 (Fig. 3b and 3c) reached their peaks slightly later than cell 1 (Fig. 3a). The magnitude of the responses in the three cells differed significantly: cells 1, 2 and 3 peaked at 300 nM, 100 nM and 200 nM calcium, corresponding to increases of 230, 30 and 90 nM calcium respectively. A second wash removed the ATP, returning the calcium levels to near initial values for all three cells. The addition of 1 μM Br-A23187, a non-fluorescent calcium ionophore [27], served to again increase calcium levels. It is interesting to note that the maximum ratio values observed following exposure to the ionophore reached only 60–70% of their R$_{max}$ values and in cells 1 and 2 did not reach levels stimulated during

the initial ATP addition. Additionally the cells appeared to regulate their calcium levels in the continued presence of the ionophore, as the calcium levels settle at a steady, albeit elevated, value after approximately 100 s. This result suggests that we have not overloaded the capacities of the cells to pump or store free calcium. A final addition of 1 μM Br-A23187 and 2 mM MnCl$_2$ was used to quench the Fura-2 fluorescence by allowing the entry of substantial amounts of Mn^{2+} into the cells. Approximately 80% of the fluorescence was quenched by this treatment. As Mn^{2+} quenches only the Fura–2 anion and not Fura–2/AM, the remaining cell-associated fluorescence is due to non-hydrolyzed or partially hydrolyzed Fura–2/AM or to Fura–2 free acid that is isolated from the Mn^{2+}. The former is more likely since the fluorescence ratio R drops to a low value, characteristic of the spectral response of Fura–2/AM [28].

To examine the kinetics of the calcium transients in single cells in more detail, the response of a single cell to ATP was examined by simultaneously using the frame transfer, subarray and binning capabilities of the imaging system. The cell shown in Plate 9 was imaged in a 200 x 292 pixel subarray with 2 x 2 binning, giving a final image size of 100 x 146 pixels. The cell was exposed for 500 ms at 334 nm and 50 ms at 365 nm, and pairs of images were collected approximately every 3 s. Although the image has been binned, note that cellular detail, including thin processes, are clearly visible. In Figure 4a, the corresponding plot of calcium concentration versus time is given. The calcium concentration increased rapidly from a starting level of approximately 80 nM to a peak of 840 nM upon addition of 50 μM ATP and then returns to a slightly elevated calcium level of 130 nM over the next minute. The speed of data collection allows us to examine the calcium transients in more detail than for the data of Figure 3. We note that the decrease in calcium concentration is not well characterised by simple exponential decay; this has been observed in many other cells as well (data not shown). A slight secondary rise in calcium at 100 s is also resolved. The removal of ATP from the extracellular medium causes the intracellular free calcium concentration to fall to slightly lower than its initial value. A second addition of 50 μM ATP

Table 1 Calcium levels in various regions of an individual smooth muscle cell

Region examined (Number of pixels in region)	Calcium level (nM)		
	Resting*	First peak	Second peak
Whole cell (1856)	81.2 ± 0.4	835	339
All peripheral extensions (363)	69.4 ± 1.8	709	338
Bottom lamellepodium (231)	55.7 ± 2.8	589	294
Long extension, top left (80)	76.1 ± 3.8	388	209
Cell interior, non-lamellepodial (1361)	86.2 ± 0.3	904	354
Upper half of cell interior (863)	89.7 ± 0.2	1062	399
Lower half of cell interior (613)	78.3 ± 0.6	702	295

* Four data points before the first ATP addition were averaged to obtain the resting calcium level. The result is expressed as mean ± standard error

at 160 s stimulates a second dramatic rise in calcium concentration. A desensitisation of the ATP response is again suggested, as the second peak has a maximum of only 350 nM. The fall from the elevated calcium level to a steady and lower level again occurs in roughly one minute and is clearly not characterised by a single exponential.

To address the spatial dependence of the calcium response to ATP, the cell of Plate 9 and Figure 4a was examined in greater detail. Seven separate regions of the cell were selected and analysed. The temporal dependence of the calcium response was identical from region to region within the cell in that the initiation of both increases in $[Ca^{2+}]_i$ and the times at which a peak was reached were the same (not shown). However, as may be seen in Plate 9, the resting and peak $[Ca^{2+}]_i$ levels varied from point to point (see Table 1).

The results of a similar experiment are shown in Figure 4b. Pairs of images were collected approximately every 2.5 s for a subarray with a 2 x 2 binned size of 44 x 146 pixels. The addition of 50 μM ATP stimulated a rise in calcium concentration from 100 to 1800 nM, followed by a return to a slightly elevated level. As in Figure 4a there is a second minor calcium transient occurring after the first.

The data shown in Figure 5 are the result of an experiment on a field containing 2 cells. Frame transfer 2 x 2 binned images were collected approximately every 3.5 s. Cell 2 responds in a fashion similar to the cells of Figure 4: $[Ca^{2+}]_i$ rises rapidly from approximately 100 nM to 530 nM calcium upon addition of 50 μM ATP, followed by

a decrease, a strong secondary peak and a second decrease to nearly the initial concentration. As in Figures 3 and 4a, a second addition of 50 μM ATP stimulates a less dramatic rise in calcium; in this cell, however, the secondary peak following this second response is nearly equal in height to the response itself. The addition of 1 μM Br-A23187 stimulated a rise in calcium and then a decrease to a steady elevated level; the simultaneous addition of 1 μM Br-A23187 and 2 mM $MnCl_2$ quenched fluorescence and depressed ratio values as in Figure 3. After both the first and second ATP stimulations, a second peak of $[Ca^{2+}]_i$ delayed about 100 s after the initial response was seen in this cell.

The calcium levels of cell 1 in Figure 5 have quite a different character than those of cell 2. The calcium concentration in this cell before stimulation is elevated to approximately 300 nM. Stimulated increases in the calcium concentration are observed for cell 1 in response to both ATP and Br-A23187; the magnitude of the increases in cell 1 are less than in cell 2 for the first addition of ATP, greater than in cell 2 for the second addition of ATP, and approximately the same in the two cells for the addition of Br-A23187. The data for cell 1 appear to be much noisier than for cell 2 or for the cells shown in Figures 3–5 and Plate 9. An examination of the original data (not shown) indicates that the noisy cell is at least as bright as cell 2 for both wavelengths of illumination; thus the noise is not due to a low signal to noise ratio for cell 1 as compared with cell 2 (see Discussion).

In Figures 3–5 $[Ca^{2+}]_i$ transients subsequent to the initial response spike can be discerned in several
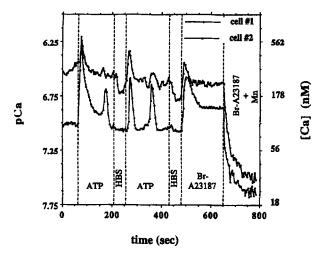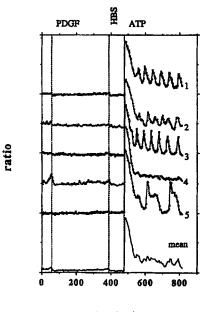
Fig. 5 Variations in calcium concentration with time in response to ATP and ionophore for two cells in the same field. Agents were added or removed at times indicated by the vertical dashed lines. Agonist concentrations: ATP, 50 μM; Br-A23187, 1 μM; MnCl₂, 2 mM. Images were collected using frame transfer, subarray and binning capabilities

individual cells. That these subsequent transients persist repetitively is shown in Figure 6 which demonstrates that SMCs respond to ATP stimulation both by a rapid $[Ca^{2+}]_i$ transient and a sustained train of rises in $[Ca^{2+}]_i$ which have been termed oscillations in studies of other cell types [12, 13, 29]. The data in Figure 6 are from a 194 x 146 pixel field; exposure times of 700 ms at 334 nm and 90 ms at 365 nm were used. Frame transfer, 2 x 2 binned images were collected approximately every 2.3 s. The fluorescence ratio R, normalised such that $R_{prestimulus} = 1$, is plotted versus time. As noted elsewhere [2] and as stated later in the Discussion section, the 334/365 image pair produces ratio values which are nearly linear with pCa over the range of 100 nM to 1 μM. Thus the R values reported here are representative of changes in pCa in the cells. The lack of response of the cells to platelet derived growth factor (PDGF-BB, recombinant from E. coli, Bachem Inc., Torrance, CA, USA), is likely due to the slowness of recovery of PDGF receptors on these cells after trypsinisation; the flatness of the traces indicates the stability of $[Ca^{2+}]_i$ in the cells prior to the ATP response. An injection of 50 μM ATP at 476 s stimulated $[Ca^{2+}]_i$ increases in all 5 cells. The $[Ca^{2+}]_i$ levels in 4 of the 5 cells then began to oscillate: the oscillation

Fig. 6 Responses of five SMCs exposed to 75 ng/ml PDGF followed by 50 μM ATP. The PDGF was washed from the cell chamber at t = 385 s. Cell responses are plotted as fluorescence ratio (R = F₃₃₄/F₃₆₅) which is proportional to pCa (see Discussion), and are shifted vertically for clarity. Variation of R over the microscope field has been corrected. The average response of the five cells is shown by the bottom trace labeled 'mean'

frequencies in cells 1, 2, 3 and 5 are, respectively, 1.3 min⁻¹, 1.4 min⁻¹, 1.2 min⁻¹ and 0.45 min⁻¹. Although the initial or primary calcium peaks of all 5 cells are synchronous to within the time resolution of the experiment, the ensuing oscillations are asynchronous from cell to cell as shown by the bottom trace in Figure 6 which is the average of the 5 cell responses. Finally, the oscillations do not show all the same characteristics. Cells 1 and 3 show highly regular and simple oscillations, cell 2 demonstrates less regular oscillations and cell 5 shows oscillations with an irregular shape. One of the cells, (cell 4), fails entirely to oscillate.

Discussion

Imaging system

One cell in Figure 5 has a much higher resting $[Ca^{2+}]_i$ than other cells shown in this report. We

find that approximately 20% of the cells we have observed (of a total >150) have significantly elevated resting $[Ca^{2+}]_i$ similar to that of cell 1 of Figure 5. In every case, the fluctuations of measured $[Ca^{2+}]_i$ about its mean value are a few times more than those in cells with lower 'normal' resting $[Ca^{2+}]_i$. In order to determine whether these fluctuations are due to the cells themselves, or to the measurement technique, we have analysed the dependence of fluorescence ratio, sensitivity and relative noise versus pCa for Fura–2 determination of $[Ca^{2+}]_i$. Since the wavelength pair (334/365 nm) we employ for Fura–2 ratio imaging differs from the more commonly used wavelength pair (340/380 nm), we additionally compare these properties for the two wavelength pairs. As can be readily discerned by examining the excitation spectra for Fura–2 at various Ca^{2+} concentrations [26], the absolute value of ratio R for the 334/365 nm wavelength pair is always less than that for 340/380 nm at any value of pCa. Figure 7a is a plot of R versus pCa for both wavelength pairs, normalised such that R = 1 at $[Ca^{2+}] = K_d$ for both curves. This normalisation is equivalent to adjusting fluorescence exposure time or excitation intensity to produce equivalent brightness images at $[Ca^{2+}]$ = 224 nM and thus allows us to compare the two wavelength pairs on the same scale. Over the range of pCa typically encountered in cells, 100 nM to 1 μM, the 334/365 ratio is nearly linear with pCa while 340/380 is less so (inset, Fig. 7a). Thus the grey levels of 334/365 ratio images are reasonably representative of pCa, allowing one to estimate the calcium response of a cell with only three image computation steps (two subtractions and one division). The sensitivity of the response of R to a change in pCa ($\delta R/\delta pCa$) for the two wavelength pairs is not shown in Figure 7b. The sensitivity of the 340/380 pair is greater than that for 334/365 over most of the physiological range of pCa. Note that the peak sensitivity of the 334/365 pair is in the middle of the physiological range (430 nM) while that for the 340/380 range is at the high end (2400 nM).

For a single measurement, the relative uncertainty of the ratio in any given pixel is the sum of relative uncertainties in the numerator and denominator image pixels, it is straightforward to derive the

expression for the uncertainty in R:

$$\frac{\Delta R}{R} = (\frac{\Delta F}{f_{D,min}}) (K_d + [Ca^{2+}]) \cdot$$

$$\beta \{ (\beta K_d R_{min} + [Ca^{2+}]R_{max})^{-1} + (\beta K_d + [Ca^{2+}])^{-1} \}$$

where ΔR is the absolute uncertainty (or noise) in R, ΔF is the typical noise level in a pixel, $f_{d,min}$ is the intensity of fluorescence excited at the denominator wavelength in the absence of calcium, and R_{max}, R_{min}, β, and K_d are as defined earlier. For a determination of the mean $[Ca^{2+}]_i$ based on multiple data samples the standard deviation of R follows a more complicated expression. Our expression is the upper bound to the standard deviation. Fluctuations in the number of calcium ions in the region represented by a pixel as well as diffusive or Ca^{2+}-binding fluctuations in Fura–2 fluorescence are assumed to occur on a timescale much shorter than our shortest exposure time, 50 ms. For our images, the dominant contribution to pixel grey level uncertainty is camera noise. $\Delta F/F$ is of the order of 0.05 for the brightest regions in the cell. Figure 7c shows the relative uncertainty in R as a function of pCa for the two wavelength pairs, normalised so that $f_{365,min} = f_{380,min}$ at $[Ca^{2+}]_i = K_d$, again to allow us to compare the two wavelength pairs at the same scale. The relative noise for the 334/365 image pair decreases from low to high $[Ca^{2+}]_i$, which, in combination with the dependence of R on pCa for this wavelength pair, indicates that the absolute uncertainty in R is relatively constant over the whole range of pCa. The most important measurement uncertainty is shown in Figure 7d in which relative fluctuations were measured pCa ($\Delta pCa/pCa$) are plotted versus actual pCa. We have included in this plot contributions due to fluctuations in all the measured parameters R, β, R_{min} and R_{max}. As the cell images which are used to calculate R are ten times dimmer than those used to calculate β, R_{min} and R_{max} for our experiments, the relative fluctuations in the calibration images are ten fold lower than those in the cell images. Again the relative uncertainty for the 340/380 wavelength pair has been normalised to that for 334/365. $\Delta pCa/pCa$ is lower for the 340/380 wavelength pair except over the pCa range from 6.6–6.9 (126–250 nM). Note that the relative uncertainty for the
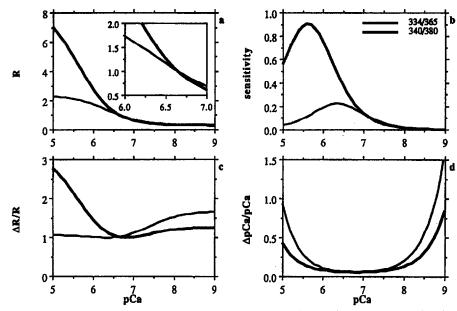
Fig. 7 Ratio (a), $\delta R/\delta pCa$ (b), $\Delta R/R$ (c) and $\Delta pCa/pCa$ vs pCa for the 334/365 nm and 340/380 nm wavelength pairs. Spectral data were taken from [25] to obtain R_{min}, R_{max} and β. No correction for viscosity was made. The plot of $\Delta R/R$ (c) assumes $\Delta F/f_{D,min} = 1$, i.e. corrected values of $\Delta R/R$ for any given pixel must be multiplied by the measured $\Delta F/f_{D,min}$. In the plot of $\Delta pCa/pCa$ (d), the 340/380 nm wavelength curve has been normalised to the 334/365 nm curve at the point at which $pCa = pK_d$. $\Delta F/f_{D,min} = 0.005$ for the images generating R while $\Delta F/f_{D,min} = 0.005$ for the images generating R_{min}, R_{max} and β. See text for details

334/365 wavelength pair is only 8% greater at pCa = 6.5 than at pCa = 7.0. Using this fact to interpret the data of Figure 5, it appears that the fluctuations in the upper trace (cell 1) are not due to instrumental noise. As stated earlier, the absolute signal detected for cell 1 was no less than that detected for cell 2, ruling out a difference in the signal/noise ratio between the two cells as an explanation. Thus it appears that the fluctuations associated with cell 1 arise from intrinsic fluctuations in $[Ca^{2+}]_i$; the cellular basis of this calcium noise is not apparent.

The operation of the CCD in one or more specialised modes offers a variety of options to the user. Collection of a single image at full resolution on the CCD requires approximately 1.5 s for readout and image storage. Because fluorescence ratio imaging requires two separate images of the same field, each corresponding to a different excitation wavelength, operation of the CCD in this mode would require at least 3.0 s for the collection of data to compute one ratio image, exclusive of actual exposure times. For this reason, it is often desirable to collect data on only one portion of the entire field, a subarray. The clear advantages, particularly

for the collection of data to form ratio images, are faster interframe, readout and storage times. Binning the charge as it is collected from the CCD also offers the advantage of faster image transfer times; this advantage couples with that of shorter exposure times for a fixed image brightness. The use of this technique is particularly helpful for images of Ca^{2+} transients in SMC, for full frame unbinned images require a total exposure time in the order of 2 s. Although the spatial resolution of the binned image is reduced in comparison with an unbinned image, individual cells and some intracellular structure are still distinguishable even with 3 x 3 binning.

Operation of the CCD in frame transfer mode, employing it simultaneously as a photoelectron storage and collection device, is particularly suited to Fura-2 ratio imaging because both images needed for the ratio are collected with minimal time between images. Errors due to temporal misregistry between numerator and denominator images are greatest when Ca^{2+} is rapidly changing or when cells move rapidly. For frame transfer imaging with our system, the predominant cause of temporal misregistry is the exposure time of the 334 nm image.

Ca^{2+} transients in SMC

In an earlier study, Tawada and co-workers [20] demonstrated ATP-induced calcium transients in suspensions of cultured smooth muscle cells from rat aorta. We extend those observations to individual cultured swine aortic smooth muscle cells attached to a substrate, and examine detailed kinetics of the calcium transient. Rapid imaging of cells, taking pairs of images every 2–3 s, allows us to resolve features in the $[Ca^{2+}]_i$ response curves that are not readily apparent with slower imaging. For example, the data on the decline of the ATP-induced calcium transient shown in Figure 3 give no indication of the subtle features we note with the data of Figures 4 and 5. The slight secondary calcium transients observed in Figures 4 and 5 would be missed entirely if pairs of images were collected more slowly. The asynchronous sustained oscillations of $[Ca^{2+}]_i$ shown in Figure 6 would appear as noise with lower time resolution data collection. The pattern of these oscillations varies widely from cell to cell as has been reported for other cells [29, 30]; the data reported in Figure 6 are typical of our observations of more than 150 SMCs. We find that most (~70–80%) of the cells with resting levels of $[Ca^{2+}]_i$ near 100 nM display calcium oscillations after the ATP-stimulated transient when observation times extend for 2 minutes or longer, and that the oscillations require the continued presence of the stimulant. A more detailed study of these oscillations is in progress.

The data shown here support the postulate that desensitisation of the ATP-induced calcium response occurs with continued exposure to ATP and extracellular calcium. After an initial exposure of the cells to ATP for approximately 100–200 s and a brief (50–150 s) wash, an identical dose of ATP produces a significantly decreased calcium response. Benham and Tsien [21] have shown that ATP-activated Ca^{2+} channels in aortic smooth muscle inactivate within ~2 s after application of 1 μM ATP. As the decline of the whole-cell Ca^{2+} response to ATP we find has a considerably longer time course than 2 s, either a second mode of desensitization or altered ATP-activated Ca^{2+} channel activity in our cells is indicated. The former is supported by the fact that stimulation of SMC with

ATP in Ca^{2+}-free, EGTA-containing HBS produces the initial $[Ca^{2+}]_i$ transient (not shown), implicating release of calcium from intracellular stores as the primary source of the initial rise in $[Ca^{2+}]_i$.

Elevated intracellular calcium levels are also observed after the addition of Br-A23187. The fluorescence ratio in these cells does not, however, reach R_{max} levels and, in the cells examined, this response is less in magnitude than the initial response to ATP. The subsequent decline of calcium levels to a steady though elevated level suggests that SMCs regulate their calcium levels to some degree in the continued presence of the ionophore. The addition of Br-A23187 together with Mn^{2+} leads to a quenching of Fura–2 fluorescence, suggesting that Mn^{2+} is entering ion channels opened by the ionophore [3]. The fact that not all of the cell-associated fluorescence is quenched by this treatment and that the ratio values of the cells drop dramatically when Mn^{2+} is added (Figs 3, 6) indicates that not all of the Fura–2/AM is completely hydrolysed by SMCs. This result complicates our measurement of $[Ca^{2+}]_i$ since the contribution of Fura–2/AM fluorescence tends to artifactually depress measured $[Ca^{2+}]_i$. Since the Fura–2/AM may redistribute within a cell during our measurement interval, we have chosen not to attempt a further correction for this artifact.

Careful examination of Plate 9 shows that the apparent distribution of $[Ca^{2+}]_i$ is heterogeneous, even in unstimulated cells. It is quite likely that some of the Fura–2 anion is entrapped within organelles such as sarcoplasmic reticulum and mitochondria and that these regions report higher $[Ca^{2+}]_i$ than does the cytosol. A recent report [25] indicates that interaction of Fura–2 with intracellular macromolecules can greatly affect both K_d and the spectral properties of Fura–2. This fact, coupled with an uncertainty in the true intracellular viscosity of an individual cell cast doubt on the accuracy of the absolute calibration of calcium that we report. However, the details of kinetics described here are not significantly affected by such uncertainties.

In conclusion, the charge-coupled device imaging system we describe is well suited to the rapid and accurate ratiometric imaging of $[Ca^{2+}]_i$ in individual cells and of multiple cells in the same field of view. The data reported here describe subtle features in

the calcium transients in SMC exposed to ATP and Br-A23187.

Acknowledgements

References

1. Pandol SJ. Schoeffield MS. Fimmel CJ. Muallem S. (1987) The agonist-sensitive calcium pool in the pancreatic acinar cell: Activation of plasma membrane Ca^{2+} influx mechanism. J. Biol. Chem., 262, 16963-16968.

2. Gonzalez FA. Gross DJ. Heppel LA. Webb WW. (1988) Studies on the increase in cytosolic free calcium induced by epidermal growth factor, serum and nucleotides in individual A431 cells. J. Cell Physiol., 135, 269-276.

3. Hallam TJ. Jacob R. Merritt JE. (1988) Evidence that agonists stimulate bivalent-cation influx into human endothelial cells. Biochem. J., 255, 179-184.

4. Merritt JE. Hallam TJ. (1988) Platelets and parotid acinar cells have different mechanisms for agonist-stimulated divalent cation entry. J. Biol. Chem., 263, 6161-6164.

5. Sage SO. Rink TJ. (1987) The kinetics of changes in intracellular calcium concentration in Fura-2-loaded human platelets. J. Biol. Chem., 262, 16364-16369.

6. Gonzalez FA. Heppel LA. Gross DJ. Webb WW. Parries G. (1988) The rapid desensitization of receptors for platelet derived growth factor, bradykinin, and ATP: Studies on individual cells using quantitative digital video fluorescence microscopy. Biochem. Biophys. Res. Commun., 151, 1205-1212.

7. Sommerville LE. Hartshorne DJ. (1986) Intracellular calcium and smooth muscle contraction. Cell Calcium, 7, 353-364.

8. Bond M. Kitazawa T. Somlyo AP. Somlyo AV. (1984) Release and recycling of calcium by the sarcoplasmic reticulum in guinea-pig portal vein smooth muscle. J. Physiol., 355, 677-695.

9. Somlyo AV. Bond M. Somlyo AP. Scarpa A (1985) Inositol trisphosphate-induced calcium release and contraction in vascular smooth muscle. Proc. Natl Acad. Sci. USA, 82, 5231-5235.

10. Tsien RY. Rink TJ. Poenie M. (1985) Measurement of cytosolic free Ca^{2+} in individual small cells using fluorescence microscopy with dual excitation wavelengths. Cell Calcium, 6, 145-157.

11. Williams DA. Fogarty KE. Tsien RY. Fay FS. (1985) Calcium gradients in single smooth muscle cells revealed by the digital imaging microscope using Fura-2. Nature, 318, 558-561.

12. Jacob R. Merritt JE. Hallam TJ. Rink RJ. (1988) Repetitive spikes in cytoplasmic calcium evoked by histamine in human endothelial cells. Nature, 335, 40-45.

13. Ambler SK. Poenie M. Tsien RY. Taylor P. (1988) Agonist-stimulated oscillations and cycling of intracellular free calcium in individual cultured muscle cells. J. Biol

Chem., 263, 1952-1959.

14. Hiraoka Y. Sedat JW. Agard DA. (1987) The use of a charge-coupled device for quantitative optical microscopy of biological structures. Science, 238, 36-41.

15. Connor JA. (1988) Fluorescence imaging applied to the measurement of Ca^{2+} in mammalian neurons. In: Grinnel AD. Armstrong D. Jackson MB. eds. Calcium and ion channel modulation. New York, Plenum, pp. 395-406.

16. Gordon JL. (1986) Extracellular ATP: effects, sources, and fate. Biochem. J., 233, 309-319.

17. Burnstock G. Kennedy C. (1986) A dual function for adenosine 5'-triphosphate in the regulation of vascular tone. Circ. Res., 58, 319-330.

18. Ugurbil K. Holmsen H. (1981) Nucleotide compartmentalization: Radioisotopic and nuclear magnetic resonance studies. In: Gordon JL. ed. Platelets in biology and pathology. Amsterdam, Elsevier, pp. 146-147.

19. Slakey LL. (1985) Extracellular nucleotide hydrolysis and integration of signalling. In: Lands WEM. ed. Biochemistry of arachidonic acid metabolism. Boston, Martinus Nijhoff, pp. 323-341.

20. Tawada Y. Furudawa K. Shigekawa M. (1987) ATP-induced calcium transients in cultured rat aortic smooth muscle cells. J. Biochem., 102, 1499-1509.

21. Benham CD. Tsien RW. (1987) A novel receptor-operated Ca^{2+}-permeable channel activated by ATP in smooth muscle cells. Nature, 328, 275-278.

22. Goldman SJ. Dickinson ES. Slakey LL. (1983) Effect of adenosine on synthesis and release of cyclic AMP by cultured vascular cells from swine. J. Cyclic Nucleotide Res., 9, 69-78.

23. Libby P. O'Brien KV. (1983) Culture of quiescent arterial smooth muscle cells in a defined serum-free medium. J. Cell Physiol., 115, 217-223.

24. Meltzer RJ. (1969) Spectographs and monochromators. In: Kingslake R. ed. Applied optics and optical engineering. New York, Academic Press, pp. 47-84.

25. Konishi M. Olson A. Hollingworth S. Baylor SM. (1988) Myoplasmic binding of Fura-2 investigated by steady-state fluorescence and absorbance measurements. Biophys. J., 54, 1089-1104.

26. Grynkiewicz G. Poenie M. Tsien RY. (1985) A new generation of Ca^{2+} indicators with greatly improved fluorescence properties. J. Biol. Chem., 260, 3440-3450.

27. Deber CM. Tom-Kun J. Grinstein S. (1985) Bromo-A23187: A nonfluorescent calcium ionophore for use with fluorescent probes. Anal. Biochem., 146, 349-352.

28. Scanlon M. Wiliams DA. Fay FS. (1987) A Ca^{2+}-insensitive form of Fura-2 associated with polymorphonuclear leukocytes: Assessment and accurate Ca^{2+} measurement. J. Biol. Chem., 262, 6308-6312.

29. Berridge MJ. Galione A. (1988) Cytosolic calcium oscillators. FASEB J, 2, 3074-3082.

30. Prentki M. Glennon MC. Thomas AP. Morris RL. Matschinsky FM. Corkey BE. (1988) Cell specific patterns of oscillating free Ca^{2+} in carbamylcholine-stimulated insulinoma cells. J. Biol. Chem., 263, 11044-11047.

Please send reprint requests to: Dr D. J. Gross, Department of Biochemistry and Program in Molecular and Cellular Biology, University of Massachusetts, Amherst, MA 01003, USA